This is a repository copy of *Behavior and design of cold-formed steel bolted connections subjected to combined actions*.

White Rose Research Online URL for this paper:
https://eprints.whiterose.ac.uk/181963/

Version: Accepted Version

Behavior and Design of Cold-Formed Steel Bolted Connections

Subjected to Combined Actions

Seyed Mohammad Mojtabaei[1], Jurgen Becque[2], Iman Hajirasouliha[3]

[1]*Ph.D. Researcher, Dept. of Civil and Structural Engineering, Univ. of Sheffield, Sheffield S1 3JD, UK (corresponding author). ORCID: https://orcid.org/0000-0002-4876-4857. Email:* smmojtabaei1@sheffield.ac.uk
[2]*Lecturer, Dept. of Engineering, Univ. of Cambridge, Cambridge CB2 1PZ, UK. Email:* jurgen.becque@eng.cam.ac.uk
[3]*Senior Lecturer, Dept. of Civil and Structural Engineering, Univ. of Sheffield, Sheffield S1 3JD, UK. ORCID: https://orcid.org/0000-0003 -2597-8200. Email:* i.hajirasouliha@sheffield.ac.uk

Abstract

Cold-formed steel (CFS) moment connections are often formed by bolting the webs of the connecting elements to a stiffened gusset plate, and local buckling of the web adjacent to the connection typically governs their capacity. This paper aims to study this failure mode in case the connection is subject to combined axial compression, shear and bending moment. In a first step, the case of pure compressive loading was investigated. Validated GMNIA Finite Element (FE) models were used to investigate the effects of different design variables, including the cross-sectional geometry and thickness, the bolt group configuration and the bolt group length. The results were then used to develop design equations for the compressive capacity of CFS bolted connections. In a next step, the FE models were used to assess the capacity of CFS bolted connections subject to combined bending and shear, and combined axial compression, bending and shear. Suitable interaction equations were proposed and reliability analyses were performed within the framework of both the Eurocode and the AISI standards. It was concluded that a linear equation accurately captures the interaction between bending moment and axial force, while the effects of a shear force smaller than half of the shear capacity on the bending moment capacity can be neglected.

Keywords: cold-formed steel (CFS); bolted connection; Finite Element (FE) modelling; bolt group length; reliability; interaction equations

1 Introduction

Over the past decades few materials have seen as dramatic an expansion in their range of application as cold-formed steel (CFS). Originally almost exclusively confined to secondary members (such as purlins, side rails and

cladding) in industrial buildings, CFS nowadays is a prominent building material, owing to the recognition of its multitude of advantages. An example of this development is the emergence of residential and office buildings with up to seven storeys constructed entirely out of CFS, including the load-bearing stud walls, floor systems and strap or K-bracings. In this case, the primary incentive for choosing CFS, apart from it being cost-competitive, is its unrivalled construction speed, driven by off-site fabrication which enables a panelized or even modular approach. CFS structural members characteristically exhibit high strength-to-weight ratios, which originate from using slightly higher steel grades (e.g. 450 MPa) for the initial flat plate, combined with the added benefit of work-hardening during cold-rolling, as well as from the slender make-up of the cross-section which results in advantageous cross-sectional properties despite the increased susceptibility to local and/or distortional buckling. When also accounting for their recyclability without loss of quality and their improved durability (due to their galvanized coating) CFS members can boast important sustainability credentials, an important factor in today's world and one which is only expected to increase in importance.

Over the past decades CFS has also conquered an increasingly important market share in the construction of portal frames. Portal frames are the pre-eminent structural system when large open spaces are required, for instance for sports and event centres, industrial halls, indoor markets and warehouses. Also in this area has CFS construction undergone a staggering increase in physical scale. Where early applications mainly involved short span (e.g. 5-7 m) frames composed of single lipped channels, several innovative (and often proprietary) CFS systems can nowadays provide span lengths of up to 50-60 m, where the rafters often comprise CFS trusses. In the intermediate span range columns and rafters composed of back-to-back lipped channels are very popular and they form the main focus of this paper (Fig. 1). Lipped channel sections with depths of up to 500 mm and a thickness of 4 mm are available in the UK. While span lengths of up to 25 m are theoretically within reach, they are most often limited to about 15 m, as there is still a great deal of unease among manufacturers with respect to the portal frame connections, both in terms of their rotational stiffness and their capacity, as insufficient knowledge is available. The eaves and apex connections in CFS portal frames are fundamentally different from the rigid connections typically encountered in hot-rolled frames. The CFS community is quite averse to welding, in part because the galvanizing produces heavily toxic fumes when heated, but also because of the technical difficulties in welding thin-walled elements (distortions, burn-through, etc.). A much preferred, and at the same time quick and convenient way of assembling CFS portal frames on site therefore consists of bolting the columns

2

and rafters to stiffened gusset plates ('brackets') through their webs (Fig. 1) (Lim and Nethercot, 2002). However, this arrangement requires all actions in the elements (axial force, shear and bending) to be transferred into the gusset plate by the web. As a result, localized web buckling adjacent to the gusset plate has been observed to be the governing failure mode in experimental research by Kirk (1986), Chung and Lau (1999), and Lim and Nethercot (2003), as well as in full-scale portal frame tests by Dubina et al. (2009). A comprehensive study of the phenomenon was carried out by Lim and Nethercot (2003, 2004), including four-point bending tests on apex connections, numerical studies and a proposed design equation. The design aspects of this failure mode were further explored by Lim et al. (2016), who attributed premature failure in the web to a combination of a major axis bending moment and a bimoment equal to the product of the reaction force with the distance from the web (where the reaction is introduced) to the shear centre of the individual channel. These topics were further investigated in a precursor to the current paper (Mojtabaei et al., 2020), based on parametric studies using an FE model which was first validated against the experiments by Lim and Nethercot (2003). The research pertained to CFS portal frame connections between back-to-back lipped channels under uniform bending and led to the following important conclusions:

- In doubly-symmetric sections the reduction of the cross-sectional capacity at the connection is due to the localized introduction of the load causing a shear lag effect, rather than to the workings of a bi-moment.

- The eccentricity between the web of an individual channel and its centroid is an important but previously overlooked parameter determining the connection capacity. Consequently, the equations proposed in (Lim and Nethercot, 2003) have limited scope.

- The connection capacity converges exponentially to the full cross-sectional capacity when the length of the bolt group is increased, rather than logarithmically, as previously thought.

New design equations were proposed for CFS connections transferring a uniform bending moment, taking account of the above conclusions. While this is a step in the right direction, it does not rectify the lack of design guidance for practical applications. Indeed:

- Portal frame members are never subject to uniform bending. Instead, both the columns and the rafters typically carry a combination of bending, shear and axial load.

3

- Any proposed design equations accounting for combined loading subsequently need to be verified by a reliability analysis to ensure that, when combined with prescribed safety factors, they possess the right margin of safety.

Both issues are addressed in this paper.

Numerous previous studies have focused on the tensile behaviour of eccentric bolted CFS connections, with appropriate consideration of shear lag effects. Early work in this area was conducted by Munse and Chesson (1963) on bolted and riveted tension members, and further extended by Easterling and Gonzalez (1993), who investigated welded connections, and by Kulak and Wu (1997) on the topic of bolted angle connections. Orbison et al. (2002) experimentally investigated the influence of varying the connection eccentricity and the connection length on the tensile capacity. More recently, Teh et al. (2012, 2013a, 2013b) experimentally evaluated the accuracy of the equations specified by the North American (AISI, 2007) and Australian codes (AS/NZS 4600, 2005) to determine the net section tensile capacities of CFS angles bolted at one leg, flat steel sheets and channel sections, and subsequently proposed more accurate design equations. In another relevant study Bolandim et al. (2013) performed a reliability analysis on the results of a comprehensive experimental programme on CFS bolted connections and proposed a reduced safety factor compared to the one specified by the AISI rules.

Despite this rather large body of research on the tensile capacity of eccentric CFS bolted connections, no studies could be found on their compressive capacity, where the additional complexity of local web buckling has to be accounted for. Addressing this gap in knowledge was therefore the first point of focus in the current study. The capacities of CFS bolted connections in pure compression and pure bending (obtained from previous research (Mojtabaei et al., 2020)) then formed the building blocks to study the capacity under combined actions. The influence of various parameters on the connection capacity (in particular the cross-sectional geometry and thickness, and the bolt group configuration and length) were investigated by means of detailed finite element studies, accounting for geometric and material non-linearity, imperfections, contact and non-linear bolt behaviour, after validating the model against previous experimental research. The main contribution of the study consists in presenting design interaction equations to predict the capacity of typical bolted CFS portal frame connections subject to combined bending and shear, and combined axial compression, bending and shear, validated by reliability analyses. No such equations are currently available.

It is reiterated that the scope of the investigation is limited to failure by cross-sectional instability of the connected member and that other possible failure modes pertaining to the bolts (e.g. bearing failure, shear failure of the bolts, block tear-out), the gusset plate (e.g. lateral-torsional buckling, local buckling) or the member (e.g. net section failure) are assumed to be non-governing by way of appropriate design.

2 Finite element model

Finite element (FE) modelling is a well-established tool in the analysis of CFS bolted connections (Lim and Nethercot, 2003, Lim and Nethercot, 2004, Bagheri Sabbagh et al., 2013, Bučmys et al., 2018, Mojtabaei et al., 2018, Ye et al., 2018a, Ye et al., 2019, Mojtabaei et al., 2020, Ye et al., 2020, Phan et al., 2020) and good agreement between FE predictions and the experiment has previously been reported. In this study an FE model previously developed by the authors in (Mojtabaei et al., 2020) and validated against the experiments by Lim and Nethercot (2003) was utilized to simulate the behaviour of connections in compression, combined shear and bending, and combined shear, bending and axial compression. The software package ABAQUS (2014), alongside its Python scripting interface, was employed to develop the FE models, which accounted for geometric and material non-linearity, as well as imperfections. The main features of the models are briefly summarized below.

2.1 Geometry and boundary conditions

The FE model of a typical CFS bolted connection is shown in Fig. 2 and consists of CFS back-to-back lipped channels connected to a gusset plate. A 'hard' surface-to-surface contact was defined between the channels and the gusset plate. Fully clamped (fixed) boundary conditions were applied to the end of the gusset plate. At the opposite end of the member the degrees of freedom of the nodes of the free end section were coupled to those of a reference point located at the centroid of the whole cross-section. In the case of a connection in pure compression all degrees of freedom of the reference point were restrained except for the axial (Y-) translation, which was increased in magnitude during the simulation (Fig. 2). In the case where the capacity of the connection against combined (major axis) bending and shear was investigated, an increasing horizontal Z-displacement was imposed at the reference point, while the X-displacements and the rotations about the minor principal axis and the longitudinal axis were prevented (Fig. 3a). Finally, in the most general case of a connection subject to bending, shear and compression, an axial compressive load was first applied to the reference point, followed by a second

analysis step with an imposed horizontal Z-displacement under constant axial load (Fig. 3b). The X-displacements and the rotations about the Y- and Z-axes of the reference point were again prevented.

In all loading cases the longitudinal web edges were prevented from moving out of their plane in order to prevent global instabilities of the CFS member (i.e. flexural, torsional or flexural-torsional buckling). The modelled length of the CFS member (exclusive of the connection zone) was taken as 6 times the web height h, following a sensitivity study in (Mojtabaei et al., 2020). This length is sufficient to allow shear lag effects at the connection to develop unimpeded.

2.2 Element type and material properties

A four-noded shell element with reduced integration (S4R) was used, which has three translational and three rotational degrees of freedom at each node. This element accounts for finite membrane strains and arbitrarily large rotations, and is therefore suitable for large-strain analyses and geometrically non-linear problems. It also accounts for transverse shear deformations, although these were not deemed to be important for the problem under consideration. This particular element was previously shown by various researchers to yield accurate predictions when modelling CFS thin-walled structural elements (e.g. (Becque and Rasmussen, 2009, Ye et al., 2018b, Roy et al., 2019, Ye et al., 2018c)).

Following a mesh sensitivity analysis, an appropriate mesh size was identified to be of the order of 20×20 mm^2. Further refinement of the mesh size had a negligible effect on the prediction of the connection capacity, while increasing computational time.

The stress-strain relationship of the material was modelled using a bi-linear diagram with an initial elastic modulus E=210 GPa, followed by a linear hardening range with a slope of $E/100$. This model was previously used by Haidarali and Nethercot (2011). The yield stress f_y and the Poisson's ratio v were taken as 313 MPa and 0.3, respectively (Mojtabaei et al., 2020).

2.3 Modelling of the bolts

The bolts were modelled as realistically as possible using 'discrete fastener' elements from the ABAQUS library (2014). These elements are a computationally cost-effective alternative to explicitly modelling the bolts using solid elements, especially in connections with a large number of bolts (Ye et al., 2020). Discrete fasteners make use of attachment lines between user-defined fastening points on selected faces of surfaces to create connectors.

A 'radius of influence' is assigned to each connector and the displacements and rotations of the nodes within this radius are coupled to the displacements and rotations of the fastening point in order to avoid excessive stress concentrations. A sensitivity study, varying this radius of influence between 5 mm and 30 mm, was carried out, which indicated that the results were relatively insensitive to this parameter. A value of 8 mm, equal to half the bolt shank diameter, as recommended in (Abaqus/CAE User's Manual, 2014) was adopted. Discrete fastener elements allow the actual inelastic bolt hole elongation behaviour to be incorporated into the model. In this study the bearing behaviour of the bolts was modelled using the equations proposed by Fisher (1964):

$$R_B = R_{ult}\left[1 - e^{-\mu(\delta_{br}/25.4)}\right]^{\lambda}$$ (1)

$$R_{ult} = 2.1 \cdot d \cdot t \cdot F_u$$ (2)

where δ_{br} is the bearing deformation (in mm), R_{ult} is the ultimate bearing strength, t is the web thickness, d is the bolt diameter and R_B is the bearing force. F_u is the tensile strength of the web material, while μ=5 and λ=0.55, according to Uang et al. (2010). The bolt diameter was assumed to be 16 mm. It should be noted that bolt slippage caused by bolt hole clearance was ignored in this study. The bearing behaviour of the bolts against steel plates of different thickness is shown in Fig. 4.

It should also be mentioned that the modelled load-elongation behaviour of the bolts has a profound influence on the connection deformations, but a negligible effect on the connection capacity where it is governed by web buckling (Bučmys et al., 2018). Consequently, the choices of the above parameters were not critical for this research study.

2.4 Imperfections

The bolted connections in this study failed by cross-sectional instability adjacent to the first row of bolts, while global buckling of the CFS member was prevented. Therefore, only a localized imperfection was incorporated into the model, obtained by conducting an elastic buckling analysis in ABAQUS (2014) and using the scaled first eigenmode as the shape of the initial imperfection. For cross-sections with a thickness (t) smaller than 3 mm, the local imperfection amplitude was taken as $0.34t$ and, where a distortional influence was noticeable, as $0.94t$. These values are based on the work by Schafer and Peköz (1998) and represent the 50% values of the cumulative distribution functions of experimentally measured imperfection data (which only included thicknesses below 3

mm). For cross-sections with a thickness (t) larger than 3 mm, the imperfection magnitude was instead determined using the equation proposed by Walker (1975):

$$\omega_d = 0.3t\sqrt{\frac{\sigma_{0.2\%}}{\sigma_{cr}}} = 0.3t\lambda_s \tag{3}$$

where $\sigma_{0.2\%}$ and σ_{cr} are the 0.2% proof stress of the material and the elastic critical local/distortional buckling stress of the cross-section, respectively, and λ_s is the cross-sectional slenderness, given by:

$$\lambda_s = \sqrt{f_y / \sigma_{cr}} \tag{4}$$

The elastic buckling stress σ_{cr} can be computed using software such as CUFSM (Li and Schafer, 2010), which is based on the Finite Strip Method.

It should also be mentioned that the imperfection sensitivity of the failure mode under consideration (i.e. localized web buckling) was found in a previous study (Mojtabaei et al., 2020) to be very moderate.

2.5 Validation

The FE model presented in the previous sections was validated against experimental results by Lim and Nethercot (2003), who subjected CFS bolted connections to a state of pure bending. The specimens were composed of back-to-back lipped channels and all connections failed by local buckling of the web. The complete details of this validation process are documented in (Mojtabaei et al., 2020). A summary of the results is provided in Table 1, where l_b is the length of the bolt group, h is the depth of the cross-section, M_{max}^{exp} is the experimentally determined moment capacity of the connection and M_{max}^{FE} is the corresponding capacity obtained from the FE models. It is seen that the predictive capability of the model can be judged as very effective, since the average ratio of the FE predicted capacity to the experimental result is 1.02, with a standard deviation of 0.018.

3 Connections subject to pure compression

3.1 Methodology

The behaviour and capacity of a range of different CFS bolted connections subject to pure compressive loading were investigated using the developed FE models. The following parameters were varied in this study: (a) the cross-sectional dimensions, (b) the cross-section thickness, (c) the bolt group length, and (d) the bolt group

8

configuration. Conventional back-to-back lipped channel sections with five different sets of dimensions were considered, as shown in Fig. 5. They were selected to provide a wide range of eccentricities (X), calculated from the centroid of a single channel to the web centreline (see Table 2). It was previously demonstrated that this parameter has a crucial influence on the severity of the shear lag effect in the connection (Mojtabaei et al., 2020). Four different wall thicknesses t=1, 2, 4 and 6 mm were used for the channels, to offer a range of different web slenderness values λ_w ($\lambda_w = h/t$, where h is the web height), as listed in Table 2. Three rectangular bolt array configurations (2x2, 3x3 and 4x4 bolts) with 11 different lengths l_b were considered. The length l_b was defined as the distance between the outer bolt rows (Fig. 6) and values of l_b/h ranging from 0.5 to 3.0 in intervals of 0.25 were studied. The height of the bolt group was defined by the constant ratio $h_b/h = 0.8$ (Fig. 6) for all connections.

Since a large number of connection models were needed to consider all combinations of the selected design variables (660 in total), the ABAQUS Python scripting interface (Abaqus/CAE User's Manual, 2014), which is an extension of the Python object-oriented programming language, was used.

3.2 Results

Cross-sectional instability originating in the web was observed to be the governing failure mode in all FE models. Fig. 7 shows a typical connection at failure.

The compressive capacity of the CFS member at the connection was compared to the full cross-sectional capacity of the member (P_u) for each configuration. In order to determine the latter, additional FE models were constructed to simulate stub column tests. These models were similar in features to the models previously introduced in Section 2, in particular with respect to the element type and size, the material model and the imperfections. Overall buckling was again prevented by restraining the out-of-plane displacements of the web edges. However, the bolted connection was omitted from the model, with the bottom end of the column stub instead fixed against all displacements. An example of these FE models is depicted in Fig. 8. The length of the column stub was taken as three times the distortional buckle half-wavelength, calculated using the CUFSM (Li and Schafer, 2010) software, as suggested by Shifferaw and Schafer (2012). The resulting cross-sectional capacities P_u are listed in Table 2.

The axial compressive capacity of a CFS bolted connection (P_c) was related to P_u through the following equation:

$$P_c = RP_u \tag{5}$$

where R is a reduction factor applied to the cross-sectional compressive capacity to account for the fact that local web buckling adjacent to the connection under a non-uniform stress distribution influenced by shear lag may prevent the full cross-sectional capacity from being reached. R was assumed to be a function of the studied variables, namely the bolt group length l_b, the bolt group configuration and the cross-sectional geometry through the eccentricity X, the thickness t and the web slenderness value $\lambda_w = h/t$.

The R values resulting from the 660 FE simulations covering all possible combinations of the design parameters (including 5 cross-sections, 4 thicknesses, 3 bolt group arrays and 11 bolt group lengths) are graphically presented in Figs. 9-11 for a 2×2, 3×3 and 4×4 bolt group, respectively. These graphs emphasize the importance of the bolt group length l_b, with the capacity of the CFS member converging to the full cross-sectional capacity as l_b increases. This convergence is exponential, as can be seen when plotting ln(1-R) against l_b/h. This is illustrated in Fig. 12 for the data pertaining to a 4×4 bolt group. A 'fan' of straight lines is thus obtained, which appear to all intersect the vertical axis at approximately the same ordinate. This suggests that an equation of the following form can be used to fit the data:

$$R = 1 - Ae^{\left(\frac{l_b}{h}\right).S} \tag{6}$$

where A is a constant and S is the slope of the lines in Fig. 12. The slopes S of the various lines are plotted as a function of the dimensionless variable t/X for the data related to the 4×4 bolt group in Fig. 13a. It is seen that the trend lines for the various cross-sectional geometries are approximately parallel, but their point of intersection S_0 with the vertical S-axis differs. Given that the various cross-sections have a different eccentricity X, as well as a different web depth h, S_0 is plotted against h/X in Fig. 13b. It is concluded that both variables are proportional. This reveals the following equation for the slope S:

$$S = -B\frac{h}{X} - C\frac{t}{X} \tag{7}$$

where B and C are (positive) constants. Substituting Eq. (7) into Eq. (6) yields:

$$R = 1 - Ae^{-\left(\frac{l_b}{X}\right)\left(B+C\frac{t}{h}\right)} \tag{8}$$

Eq. (8) shows that the reduction factor R is a function of l_b/X (rather than l_b/h) and the web slenderness h/t. This is not entirely surprising, since the AISI (AISI S100-12) design guidelines for eccentric bolted connections in tension identify l_b/X as the parameter controlling their capacity. In addition, since connections in compression are susceptible to local buckling of the web, the web slenderness h/t appears in the equation.

The constants A, B and C in Eq. (8) were determined using a genetic algorithm optimization process in Matlab (Mathworks, 2015) in order to minimize the standard deviation of the ratio R_{pred}/R_{FE} (where R_{pred} follows from Eq. 8 and R_{FE} is the value determined from the FE models). The optimization was carried out for each bolt group configuration separately. The resulting equations are as follows and their statistical indicators are presented in Table 3:

$$R = 1 - 0.39e^{\left(\frac{-l_b}{X}\right)\left(0.053+1.074\left(\frac{t}{h}\right)\right)} \tag{9}$$

$$R = 1 - 0.46e^{\left(\frac{-l_b}{X}\right)\left(0.085+2.577\left(\frac{t}{h}\right)\right)} \tag{10}$$

$$R = 1 - 0.51e^{\left(\frac{-l_b}{X}\right)\left(0.097+3.571\left(\frac{t}{h}\right)\right)} \tag{11}$$

When compared to the FE simulations, the average ratio of the predicted capacity to the FE result is very close to 1.0 for each of the bolt group configurations, with a typical standard deviation of only 0.03. A graphical comparison is also provided in Figs. 9-11. Eqs. (10) and (11) lead to nearly identical predictions, while the predictions of Eq. (9) are slightly lower. An optimized data fitting applied to the complete data set including all bolt group configurations (2×2, 3×3 and 4×4), in a similar way as carried out for the individual ones, led to the following alternative equation for R:

$$R = 1 - 0.44e^{\left[\left(\frac{-l_b}{X}\right)\left(0.072+2.465\left(\frac{t}{h}\right)\right)\right]} \tag{12}$$

The average ratio of the capacity predicted by Eq. (12) to the FE result is 1.005 with a standard deviation of 0.03.

3.3 Cross-sectional stress profiles

In order to shed more light on the phenomena at hand, Fig. 14 presents the longitudinal stress profile over the cross-section for various bolt group lengths, cross-sectional shapes and thicknesses. The stress profiles were

extracted from the FE model in the initial pre-buckled elastic range of loading and pertain to the cross-section in the CFS member at the end of the gusset plate. This cross-section was located a distance of $1.5d$ away from the first bolt row (where d is the diameter of the bolt) and is representative of the location of failure. All results relate to a 3×3 bolt group.

When comparing the stress profiles for a bolt group length $l_b = 0.5h$ to those for $l_b = 3h$ a clear conclusion emerges across all geometries and thicknesses: a much more pronounced shear lag effect is present for the short bolt groups, with the flange tips and lips carrying significantly less stress than the web-flange junction. Within each cross-section a higher thickness leads to a more uniform stress distribution in the flanges and lips, although this improvement is less pronounced in cross-sections with a higher eccentricity (Ch.4 and Ch.5) and for short bolt groups. For the thickest sections (t = 6 mm) and longest bolt group ($l_b = 3h$) the stress distribution in the flanges and lips is nearly uniform. These observed trends are completely concurrent with the influence of the variables as indicated by Eq. (9-12).

It should also be noted that the stress distribution in the web of the channels actually becomes less uniform as the thickness increases (independently of the bolt group length). This can be attributed to the amplitude of the imperfection introduced into the models, which increases dramatically from 0.34 mm for $t = 1$ mm (according to the equations in (Schafer and Peköz, 1998)) to 2.04 mm for $t = 6$ mm (according to Eq. 3). This imperfection reduces the effective stiffness at the centre of the web (note that a geometrically non-linear analysis was performed), shifting the stresses towards the web-flange junction. The concentrated forces originating from the bolts, of course, also contribute to this non-uniformity.

4 Connections subject to combined bending and shear

To evaluate the capacity of bolted CFS portal frame connections subject to a combination of bending moment and shear, further FE simulations were conducted. The model previously introduced in Fig. 3a was used, where a horizontal z-displacement was imposed at the cantilever tip to achieve both major axis bending and shear at the connection. The parameters describing the configuration (i.e. the cross-sectional geometry and thickness, and the bolt group configuration and length) were again varied over the same ranges. However, with respect to the bolt group length only the boundaries of $l_b/h = 0.5$ and $l_b/h = 3$ were considered. The results are plotted in Fig. 15 in the form of an M/M_n versus V/V_n diagram. M and V are the combinations of applied bending moment and

shear causing failure, where M is calculated as the product of V with the distance from the tip of the cantilever to the location of failure (taken as the cross-section at the end of the gusset plate). M_n is the moment capacity of the CFS member at the connection in a state of pure bending and can be determined based on previous research (Mojtabaei et al., 2020):

$$M_n = R_M M_u \tag{13}$$

In Eq. (13) M_u is the cross-sectional moment capacity of the CFS member and R_M is a reduction factor accounting for the effects of shear lag and premature buckling of the web. R_M can be determined using the following equations:

$$R_M = 1 - 0.43 e^{-11.9(\frac{t}{x})(\frac{l_b}{h})} \qquad \text{for a 2x2 bolt group} \tag{14}$$

$$R_M = 1 - 0.40 e^{-14.9(\frac{t}{x})(\frac{l_b}{h})} \qquad \text{for a 3x3 bolt group} \tag{15}$$

$$R_M = 1 - 0.42 e^{-14.5(\frac{t}{x})(\frac{l_b}{h})} \qquad \text{for a 4x4 bolt group} \tag{16}$$

V_n is the capacity of the CFS member at the connection in pure shear. Since the web of the member naturally carries almost all of the shear, a reasonable assumption is made that the capacity of the cross-section in pure shear is unaffected by the particular method of connecting the member through the web only (a routinely implied assumption in the design of steel connections). In case the AISI (AISI S100-12, 2012) provisions are used, V_n is given by the following equations:

$$\text{if} \quad \frac{h}{t} \leq \sqrt{\frac{EK_V}{f_y}} : V_n = 0.6 f_y A_w \tag{17}$$

$$\text{if} \quad \sqrt{\frac{EK_V}{f_y}} < \frac{h}{t} \leq 1.51\sqrt{\frac{EK_V}{f_y}} : V_n = \frac{0.6\sqrt{EK_V f_y}}{h/t} A_w \tag{18}$$

$$\text{if} \quad \frac{h}{t} > 1.51\sqrt{\frac{EK_V}{f_y}} : V_n = \frac{0.904 EK_V}{(h/t)^2} A_w \tag{19}$$

where A_w is the area of the web and K_V is the shear buckling coefficient of the web. For unreinforced webs the AISI rules prescribe: K_V=5.34. In case the European EN1993-1-3 (CEN, 2005a) provisions are used, the shear resistance of the cross-section (V_n) can be determined by:

$$V_n = \frac{h}{\sin \varphi} t f_{bv} \tag{20}$$

where $\varphi = 90°$ is the slope of the web relative to the flanges and f_{bv} is the shear strength of the web considering shear buckling:

$$\text{if } \bar{\lambda}_w \leq 0.83 : f_{bv} = 0.58 f_y \tag{21}$$

$$\text{if } \bar{\lambda}_w > 0.83 : f_{bv} = \frac{0.48 f_y}{\bar{\lambda}_w} \tag{22}$$

In Eq. (22) $\bar{\lambda}_w$ is the shear slenderness, which is determined using the following equation for webs without longitudinal stiffeners:

$$\bar{\lambda}_w = 0.346 \frac{h}{t} \sqrt{\frac{f_y}{E}} \tag{23}$$

All data points resulting from the FE simulations are plotted in Fig. 15. In Fig. 15a M_n and V_n were calculated according to the AISI design rules, i.e. M_u in Eq. (13) was determined using the effective width based design rules in (CEN, 2005a) and V_n was determined from Eqs. (17-19). In Fig. 15b M_n and V_n were calculated according to EN 1993-1-3 (in particular, Eqs. (21) and (22) were used to obtain V_n). A significant difference in the distribution of the results is noticed when comparing Figs. 15a and 15b. This discrepancy can mainly be attributed to the difference in V_n values resulting from both standards. Eqs. (21) and (22) implicitly take into account the end stiffening effect resulting from the gusset plate, while the AISI equations (17-19) do not. When this effect is neglected in the Eurocode, very similar values of V_n are obtained from both standards.

After inspection of the data in Figs. 14a and 14b the following interaction equation was proposed, to be used in conjunction with either the AISI or the Eurocode provisions:

$$\left(\frac{M}{M_n} \right)^2 + \left(\frac{V}{V_n} \right)^2 = 1 \tag{24}$$

The above equation is consistent with the AISI approach for cross-sections subject to combined bending and shear in limit state design. It is seen in Figs. 14a and 14b that all data points are situated above this curve. However, in the AISI framework Eq. (24) appears to be conservative for connections subject to high shear forces. Both Figs. 14a and 14b indicate that very little reduction in moment capacity is to be expected when the shear force increases. Similar observations were made by Pham and Hancock (2012). From a physical point of view this can be explained by the fact that the bending moment stabilizes the tension zone, which impedes the development of a shear buckle over the full height of the web. The observations from the numerical simulations indicate that failure always remains flexure dominated. An alternative design approach was therefore explored, where the presence of the shear force is simply neglected in the determination of the moment resistance for connections within the considered parameter range. A reliability analysis will be carried out in Section 6 to confirm whether this approach leads to a safe design methodology.

5 Connections subject to combined compression, bending and shear

The FE model previously introduced in Fig. 3b was employed to study CFS bolted connections in beam-column members simultaneously subjected to compression, bending moment and shear force. The selected design parameters were as follows:

1)   three different levels of axial compressive load: P/P_c = 0.25, 0.5 and 0.75;

2)   three different beam-column cross-sections: Ch.1, Ch.2, and Ch.3 (see Fig. 5);

3)   four different cross-sectional thicknesses: t = 1, 2, 4 and 6 mm;

4)   three different bolt group lengths: l_b/h = 0.5, 1.5 and 3.

The FE analyses required three consecutive analysis steps:

1)   an 'Elastic Buckling' analysis to provide the shape of the imperfection;

2)   a 'Static General' analysis to incrementally apply the axial compressive load up to its final value;

3)   a 'Static General' analysis to impose a horizontal displacement at the cantilever tip in the presence of the (constant) axial compressive load.

Both analyses (2) and (3) accounted for material and geometric non-linearity.

The results of these simulations are presented in Figs. 15 and 16 in the form of M/M_n versus V/V_n interaction diagrams for various levels of axial pre-load P/P_n. P, M and V are the combinations of the applied compressive

force, moment and shear force causing failure. It is thereby noted that the bending moment M was calculated based on the applied transverse load and the distance from the end section to the location of failure (at the end of the gusset plate, a distance of $1.5d$ away from the first bolt row), and also accounted for the contribution of the axial load due to the deflection of the cantilever tip (P-Δ effect). In Fig. 16 the AISI rules were used and the axial compressive capacity of the connection P_n was calculated according to Eq. (5), in combination with Eqs. (9-11). The flexural capacity of the connection M_n was determined according to Eqs. (13-16) and the shear capapcity V_n was calculated according to Eqs. (17-19). In Fig. 17, P_u, M_u and V_n were calculated according to EN 1993-1-3 instead. Fig. 18 also presents the results as M/M_n versus P/P_n diagrams, according to the AISI rules (Fig. 18a) and the Eurocode rules (Fig. 18b).

The AISI provisions currently do not provide an interaction equation for combined axial compression, bending moment and shear force in beam-column cross-sections. While such an equation is provided by EN 1993-1-3 (CEN, 2006), its applicability to web-based connections is questionable since it relies in part on the bending moment resistance of a virtual cross-section consisting of the flanges only (which are subject to a significant shear lag effect in portal frame connections and do not fully contribute). It is also immediately seen from Figs. 15 and 16 that a quadratic interaction equation of the form:

$$\left(\frac{P}{P_n}\right)^2 + \left(\frac{M}{M_n}\right)^2 + \left(\frac{V}{V_n}\right)^2 \leq 1 \tag{25}$$

inspired by Eq. (24), is unsafe, since most of the data points are located inside the domain bound by the equation. This suggests that the interaction between axial load, bending moment and shear is clearly more detrimental than the interaction between bending moment and shear alone. From a physical point of view this comes as no surprise since the axial load not only (partly or wholly) negates the beneficial effect of the tensile zone created by bending, but also promotes local buckling of the web under combined actions. A linear interaction equation is therefore proposed instead:

$$\left(\frac{P}{P_n}\right) + \left(\frac{M}{M_n}\right) + \left(\frac{V}{V_n}\right) \leq 1 \tag{26}$$

The above equation is plotted in Figs. 15-17. It can also be observed from these diagrams that, similar to Section 4, the effect of a shear force on the bending moment capacity cannot be distinguished with confidence. Therefore,

16

an alternative design approach where the effect of a shear force is neglected, effectively transforming Eq. (26) into:

$$\left(\frac{P}{P_n}\right) + \left(\frac{M}{M_n}\right) \leq 1 \tag{27}$$

is also considered in the reliability analysis carried out in the next section of this paper.

6 Reliability analysis

The proposed design equations (Eqs. (5), (24), (26) and (27)) were subjected to reliability analyses within the frameworks of both the Eurocode (CEN, 2002) and the AISI specifications (Hsiao et al., 1988) to ensure that they provide the required level of safety when combined with the code prescribed safety factors. The reliability analyses necessarily required the consideration of various uncertainties associated with the material properties, dimensions and loading, as well as modelling uncertainties inherent in the FE analyses and the proposed equations themselves.

To ensure a sufficiently small probability of failure the reliability index β must exceed a specific target value. For new structures with a design working life of 50 years and a consequence class rated as CC2 (moderate consequences of failure), the Eurocode prescribes a reliability index of 3.8 (CEN, 2002), while the AISI specifications stipulate lower bounds of 2.5 for CFS members and 3.5 for connections (Hsiao et al., 1988). The former value of 2.5 was adopted in the AISI calculations, since failure occurs in the CFS member adjacent to the connection, rather than in the connection itself. Moreover, unlike typical connection failures such as bolt shear or block tear-out, local buckling failures generally occur with ample warning, are reasonably ductile in comparison and do not immediately compromise the integrity of the structure.

It is noted that nominal capacities are divided by a partial safety factor γ in the Eurocode approach, while in the AISI specifications they are multiplied by a resistance factor ϕ. In both cases it is assumed that the factored (design) resistance matches the factored (design) loads. The governing load combination was further assumed to be comprised of dead load D and live load L, with nominal values D_n and L_n, respectively:

$$\frac{r_n}{\gamma} = \gamma_D D_n + \gamma_L L_n \text{ (Eurocode)} \quad \text{or} \quad \phi r_n = \gamma_D D_n + \gamma_L L_n \text{ (AISI)} \tag{28}$$

In the Eurocode: γ_D=1.35 and γ_L=1.5, while in the North-American code: γ_D=1.2 and γ_L=1.6. In Eq. (28) r_n is the nominal resistance.

Based on Annex D of Eurocode 0 the design resistance r_d can be written as:

$$r_d = b_1.b_2.r_m.e^{-[k_{d,\infty}\alpha_{rt}Q_{rt}+k_{d,n1}\alpha_{\delta1}Q_{\delta1}+k_{d,n2}\alpha_{\delta2}Q_{\delta2}+0.5Q^2]}$$

(29)

where b_1 and b_2 account for model uncertainties, respectively the deviations of the resistance predicted by the design equation from the FE model, and the deviations of the FE model from the experiment. In Eq. (29) r_m is the resistance determined using the mean values of all relevant variables. In this respect the probabilistic distributions of the basic variables are listed in Table 4, based on literature data (Young and Hancock, 2001, Meza et al., 2020). According to EC 0 the target calibration level $k_{d,\infty} = \alpha_R\beta$=3.04, where α_R = 0.8. The factor $k_{d,n1}$ depends on the number of FE results the design equation is validated against, which is 660, 220 and 108, respectively, for the connections in (i) pure compression, (ii) bending and shear and (iii) compression, bending and shear. Table D2 of Eurocode 0 recommends $k_{d,n1}$= 3.04 for all the above mentioned cases. The factor $k_{d,n2}$ depends on the number of experiments used to validate the FE model, which is four (Section 2.5). Since the number of experiments is relatively low, a conservative value of $k_{d,n2}$ =11.4 is prescribed by Table D2 of Eurocode 0. The validation process in Section 2.5 also yields the factor b_2 in Eq. (29) as the slope of the least squares regression line in the M_{Test} versus M_{FE} diagram:

$$b_2 = \frac{\sum(M_{Test}.M_{FE})}{\sum(M_{FE})^2}$$

(30)

M_{Test} is the flexural capacity obtained from the experiment and M_{FE} is the corresponding capacity predicted by FE analysis (Table 1).

In the case of connections under pure compressive loading, the factor b_1 can similarly be obtained as the slope of the least squares regression line in the P_{FE} versus P_c diagram:

$$b_1 = \frac{\sum(P_c.P_{FE})}{\sum(P_c)^2}$$

(31)

where P_c and P_{FE} are the compressive capacities of the connection determined by the design equation and the FE model, respectively.

In the case of connections under combined bending moment and shear, the interaction equation contains two independent variables (i.e. M/M_n and V/V_n). This additional complexity is circumvented by using the ratio of the distances d_2/d_1 for each data point in the M/M_n vs. V/V_n diagram, as shown in Fig. 19, as a substitute for the ratio of the predicted resistance over the FE result. The same approach, using the 3D M-V-P surface defined by Eq. (26), was used for the case of combined bending moment, shear and axial compression. Eq. (31) then becomes:

$$b_1 = \frac{\sum (d_2 d_1)}{\sum (d_2)^2}$$
(32)

Eurocode 0 further requires that error terms δ_1 and δ_2 be calculated, defined as:

$$\delta_1 = \frac{P_{FE}}{b_1 P_c}$$
(33)

for the case of compression, or analogously:

$$\delta_1 = \frac{d_1}{b_1 d_2}$$
(34)

for combined actions, and:

$$\delta_2 = \frac{M_{Test}}{b_2 M_{FE}}$$
(35)

The parameters Q_{rt}, $Q_{\delta 1}$, $Q_{\delta 2}$ and Q in Eq. (29) represent the standard deviation of the resistance calculated using the proposed design equation, the standard deviations of the error terms δ_1 and δ_2 and the overall standard deviation of the resistance. They are calculated as follows:

$$Q_{rt} = \sqrt{\ln(V_{rt}^2 + 1)}$$
(36)

$$Q_{\delta 1} = \sqrt{\ln(V_{\delta 1}^2 + 1)}$$
(37)

$$Q_{\delta 2} = \sqrt{\ln(V_{\delta 2}^2 + 1)}$$
(38)

$$V_r^2 = V_{\delta 1}^2 + V_{\delta 2}^2 + V_{rt}^2$$
(39)

$$Q = \sqrt{\ln(V_r^2 + 1)}$$
(40)

where V_{rt}, $V_{\delta 1}$ and $V_{\delta 2}$ are the coefficients of variation (COVs) of the calculated resistance and the error terms δ_1 and δ_2, respectively. The Eurocode 0 guidance is to calculate V_{rt} using a Taylor series approximation, while maintaining the first term in each basic variable κ_i. The variables κ_i include in this case: t (channel thickness), h (web depth), b (flange width), c (lip width), E (modulus of elasticity) and f_y (yield stress):

$$
\begin{aligned}
V_{rt}^2 &= \frac{1}{r_m^2} \left(\sum_{i=1}^{j} \frac{\partial r}{\partial \kappa_i} \sigma_i \right)^2 \\
&= \frac{1}{r_m^2} \left[\left(\frac{\partial P_c}{\partial t} \sigma_t \right)^2 + \left(\frac{\partial P_c}{\partial h} \sigma_h \right)^2 + \left(\frac{\partial P_c}{\partial b} \sigma_b \right)^2 + \left(\frac{\partial P_c}{\partial c} \sigma_c \right)^2 + \left(\frac{\partial P_c}{\partial E} \sigma_E \right)^2 + \left(\frac{\partial P_c}{\partial f_y} \sigma_{f_y} \right)^2 \right]
\end{aligned}
\tag{41}
$$

In the above equation, σ_i is the standard deviation of the variable κ_i, obtained from Table 4. The partial derivatives in Eq. (41) were calculated using finite differences. It is noted that for the cases of combined actions, P_c in Eq. (41) was replaced by d_2.

The parameters α_{rt}, $\alpha_{\delta 1}$ and $\alpha_{\delta 2}$ featuring in Eq. (29) are weighting factors for Q_{rt}, $Q_{\delta 1}$ and $Q_{\delta 2}$, respectively, obtained as:

$$
\alpha_{rt} = \frac{Q_{rt}}{Q}
\tag{42}
$$

$$
\alpha_{\delta 1} = \frac{Q_{\delta 1}}{Q}
\tag{43}
$$

$$
\alpha_{\delta 2} = \frac{Q_{\delta 2}}{Q}
\tag{44}
$$

The partial safety factor γ was then determined as:

$$
\gamma = \frac{r_n}{r_d}
\tag{45}
$$

The calculations are summarized in Table 5. It is noted that for the case of pure compression two sets of calculations were carried out, corresponding to: (i) the case where the individual equations for different bolt group configurations (Eqs. 9-11) were employed, and (ii) the case where the general Eq. (12), applicable to all bolt group configurations, was used. An average partial safety factor γ of 1.05 was obtained in both cases. In addition,

γ=1.02 and γ=1.05 were obtained for the connections under combined bending and shear, and combined bending, shear and compression, respectively.

In addition to Table 5, and further to the observations in Sections 4 and 5, the option was explored to neglect the influence of a shear force in the design of portal frame connections altogether. Practically, this means that connections subject to bending moment and shear only have to satisfy:

$$\frac{M}{M_n} \leq 1 \tag{46}$$

and that connections subject to combined axial force, bending moment and shear can be designed using Eq. (27). The results of a reliability analysis according to the previously explained principles are listed in Table 6. It is seen that similar (and even slightly lower) safety factors are obtained compared to the ones listed in Table 5, proving that this is a viable design approach when combined with the appropriate safety factors. However, this method needs to be restricted to the parameter range considered in this study and the following condition is proposed for use in the context of the Eurocode (see Fig. 15b):

$$V \leq 0.5 V_n \tag{47}$$

Eq. (47) is consistent with the design approaches in EN 1993-1-1 (CEN, 2005b), EN 1993-1-3 (CEN, 2005a) and EN 1993-1-5 (CEN, 2006) for cross-sections subject to combined bending moment and shear.

When applying the AISI (Hsiao et al., 1988) framework the resistance factor ϕ is obtained as:

$$\phi = C_\phi (M_m F_m P_{m1} P_{m2}) e^{-\beta_0 \sqrt{V_M{}^2 + V_F{}^2 + C_{P1} V_{P1}{}^2 + C_{P2} V_{P2}{}^2 + V_Q{}^2}} \tag{48}$$

where C_ϕ=1.52 for LRFD design. Moreover, M_m=1.1 and F_m=1.0 are the mean values of the material and fabrication factors, and V_M=0.1 and V_F=0.05 are the corresponding coefficients of variation (Hsiao et al., 1988, Pham and Hancock, 2012). The professional factor P_m in the original AISI equation was substituted with the product of P_{m1} and P_{m2} in Eq. (48). P_{m1} is the mean ratio of the FE predicted capacity to the capacity determined by the proposed design equation (i.e. P_{FE}/P_c for compression and d_1/d_2 for combined actions), and P_{m2} is the mean ratio of the capacity obtained from the experiments to the corresponding FE prediction (i.e. M_{Test}/M_{FE}).

V_{p1} and V_{p2} are the COVs of P_{m1} and P_{m2}, respectively, and $V_Q = 0.21$ is the COV of the loading (Hsiao et al., 1988).

In addition, the correction factors C_P take into account the number of test samples (n), according to the equation:

$$C_P = \frac{n+1}{n} \frac{n-1}{n-3}$$ (49)

The factor C_{P1} accounts for the number of numerical simulations, which is: 660, 220 and 108 for the connections under pure compression, combined bending and shear, and combined bending, shear and compression, respectively. This results in respective values of C_{P1}=1.005, C_{P1}=1.025 and C_{P1}=1.028. The factor C_{P2} depends on the number of test results in the validation procedure and was calculated to be 3.75.

The resistance factors calculated using Eq. (48) for the proposed design equations are summarized in Table 7. It is noted that the AISI rules provide two separate methodologies to calculate the cross-sectional compressive capacity P_u in Eq. (5): the effective width concept (EW) and the Direct Strength Method (DSM). Both methods were considered when evaluating the design approach proposed for compression. The EW concept was employed when considering combined actions. It is concluded that all resistance factors exceed the AISI prescribed factors of ϕ_c = 0.85 for compression, ϕ_v = 0.95 for shear and ϕ_b = 0.95 for bending. Thus, the proposed design equations can safely be used within the AISI framework in conjunction with the usual resistance factors. In particular, neglecting the influence of shear (Eqs. 27 and 46) leads to acceptable predictions, although the range of validity of this latter approach should cautiously be restricted to:

$$33.3 \leq \frac{h}{t} \leq 300$$ (50)

7 Summary and conclusions

The focus of this paper is on the behaviour, capacity and design of CFS moment connections under combined loading (bending, shear and axial force), but limited in scope to those failing by local buckling of the web. The investigation was conducted by means of systematic parametric studies using detailed finite element models, validated against experiments.

For the case of connections subject only to compression it was found that the cross-sectional capacity of the connected member may be significantly reduced due to the presence of a shear lag effect. However, the capacity of the connected member exponentially converges to the full cross-sectional capacity with increasing values of

22

l_b/X (i.e the ratio of the bolt group length to the eccentricity of the connection) and decreasing values of the web slenderness h/t.

For the case of combined bending and shear a quadratic interaction equation was proposed. On the other hand, the interaction of axial compression with bending and shear was found to be far more detrimental and a linear interaction was instead presented. In both cases, the influence of the shear force was found to be small within the range of parameters studied. The effect of shear can be safely neglected when smaller than half of the shear capacity.

The proposed design equations were subjected to a reliability analysis within the framework of both the Eurocode and the AISI specifications. Appropriate safety factors are presented in Tables 5-7 for use in practical design.

Data Availability Statement

Data, models and software code generated as part of this study are available from the corresponding author by request. Data includes details of material properties, geometric imperfections, connector behaviour and deformations.

Acknowledgement

References

Abaqus/CAE User's Manual (2014). "version 6.14-2, USA".

AISI (2007). "Supplement No. 2 to the North American specification for the design of cold-formed steel structural members". *American Iron and Steel Institute (AISI), Washington, DC, USA*.

AISI S100-12 (2012). "North American specification for the design of cold-formed steel structural members". *American Iron and Steel Institute (AISI), Washington, DC, USA*.

AS/NZS 4600 (2005). "Coldformed steel structures, Homebush, Australia". *Standards Australia/Standards New Zealand (SA/SNZ)*.

Bagheri Sabbagh, A., Petkovski, M., Pilakoutas, K. and Mirghaderi, R. (2013). "Cyclic behaviour of bolted cold-formed steel moment connections: FE modelling including slip". *Journal of Constructional Steel Research,* 80**,** 100-108.

Becque, J. and Rasmussen, K. J. R. (2009). "A numerical investigation of local–overall interaction buckling of stainless steel lipped channel columns". *Journal of Constructional Steel Research,* 65**,** 1685-1693.

Bolandim Emerson, A., Beck André, T. and Malite, M. (2013). "Bolted Connections in Cold-Formed Steel: Reliability Analysis for Rupture in Net Section". *Journal of Structural Engineering,* 139**,** 748-756.

Bučmys, Ž., Daniūnas, A., Jaspart, J.-P. and Demonceau, J.-F. (2018). "A component method for cold-formed steel beam-to-column bolted gusset plate joints". *Thin-Walled Structures,* 123**,** 520-527.

CEN (2002). "Eurocode 0: "Basis of structural design." , European Committee for Standardization, Brussels".

CEN (2005a). "Eurocode 3: design of steel structures, part 1.3: general rules—supplementary rules for cold formed members and sheeting, in, Brussels: European Comittee for Standardization".

CEN (2005b). "Eurocode 3: Design of Steel Structures. Part 1-1: General Rules and Rules for Buildings, in, Brussels: European Comittee for Standardization".

CEN (2006). "Eurocode 3: Design of steel structures, Part 1-5: Plated structural elements, in, Brussels: European Comittee for Standardization".

Chung, K. F. and Lau, L. (1999). "Experimental investigation on bolted moment connections among cold formed steel members". *Engineering Structures,* 21**,** 898-911.

Dubina, D., Stratan, A. and Nagy, Z. (2009). "Full-scale tests on cold-formed steel pitched-roof portal frames with bolted joints". *Advanced Steel Construction,* 5**,** 175-194.

Easterling, S. W. and Gonzalez, G. L. (1993). "Shear Lag Effects in Steel Tension Members". *Engineering Journal, American Institute of Steel Construction, Inc.,* 30**,** 77-89.

Fisher, J. W. (1964). "On the Behavior of Fasteners and Plates with Holes, in, Fritz Engineering Laboratory, Department of Civil Engineering, Lehigh University".

Haidarali, M. R. and Nethercot, D. A. (2011). "Finite element modelling of cold-formed steel beams under local buckling or combined local/distortional buckling". *Thin Wall Structures,* 49**,** 1554-1562.

Hsiao, L. E., Yu, W. W. and Galambos, T. V. (1988). "AISI LRFD method for cold-formed steel structural members". *9th Int. Specialty Conf. on Cold-Formed Steel Structures*.

Kirk, P. (1986). "Design of a cold-formed section portal frame building system". *Proc. 8th International Speciality Conference on Cold-formed Steel Structures, St. Louis, MO, University of Missouri-Rolla; p.295*.

Kulak, G. L. and Wu, E. Y. (1997). "Shear Lag in Bolted Angle Tension Members". *Journal of Structural Engineering,* 123**,** 1144-1152.

Li, Z. and Schafer, B. W. (2010). "Buckling analysis of cold-formed steel members with general boundary conditions using CUFSM conventional and constrained finite strip methods". *Twentieth International Specialty Conference on Cold-Formed Steel Structures, Saint Louis, Missouri, USA*.

Lim, J. B. P., Hancock, G. J., Clifton, G. C., Pham, C. H. and Das, R. (2016). "DSM for ultimate strength of bolted moment-connections between cold-formed steel channel members". *Journal of Constructional Steel Research,* 117**,** 196-203.

Lim, J. B. P. and Nethercot, D. A. (2002). "Design and development of a general cold-formed steel portal framing system". *The Structural Engineer,* 80**,** 31-40.

Lim, J. B. P. and Nethercot, D. A. (2003). "Ultimate strength of bolted moment-connections between cold-formed steel members". *Thin Wall Structures,* 41**,** 1019-1039.

Lim, J. B. P. and Nethercot, D. A. (2004). "Stiffness prediction for bolted moment-connections between cold-formed steel members". *Journal of Constructional Steel Research,* 60**,** 85-107.

Mathworks (2015). "Matlab R2015b". *Mathworks Inc.*

Meza, F. J., Becque, J. and Hajirasouliha, I. (2020). "Experimental study of cold-formed steel built-up columns". *Thin-Walled Structures,* 149**,** 106291.

Mojtabaei, S. M., Becque, J. and Hajirasouliha, I. (2020). "Local Buckling in Cold-Formed Steel Moment-Resisting Bolted Connections: Behavior, Capacity, and Design". *Journal of Structural Engineering,* 146**,** 04020167.

Mojtabaei, S. M., Kabir, M. Z., Hajirasouliha, I. and Kargar, M. (2018). "Analytical and experimental study on the seismic performance of cold-formed steel frames". *Journal of Constructional Steel Research,* 143**,** 18-31.

Munse, W. H. and Chesson, E. J. (1963). "Riveted and bolted joints: net section design". *J. Struct. Div.,* 89(1)**,** 107-126.

Orbison James, G., Barth Karl, E. and Bartels Peter, A. (2002). "Net Section Rupture in Tension Members with Connection Eccentricity". *Journal of Structural Engineering,* 128**,** 976-985.

Pham, C. H. and Hancock, G. J. (2012). "Direct Strength Design of Cold-Formed C-Sections for Shear and Combined Actions". *Journal of Structural Engineering,* 138**,** 759-768.

Phan, D. T., Mojtabaei, S. M., Hajirasouliha, I., Lau, T. L. and Lim, J. B. P. (2020). "Design and Optimization of Cold-Formed Steel Sections in Bolted Moment Connections Considering Bimoment". *Journal of Structural Engineering,* 146**,** 04020153.

Roy, K., Mohammadjani, C. and Lim, J. B. P. (2019). "Experimental and numerical investigation into the behaviour of face-to-face built-up cold-formed steel channel sections under compression". *Thin-Walled Structures,* 134**,** 291-309.

Schafer, B. W. and Peköz, T. (1998). "Computational modeling of cold-formed steel: characterizing geometric imperfections and residual stresses". *Journal of Constructional Steel Research,* 47**,** 193-210.

Shifferaw, Y. and Schafer, B. W. (2012). "Inelastic Bending Capacity of Cold-Formed Steel Members". *Journal of Structural Engineering,* 138**,** 468-480.

Teh Lip, H. and Gilbert Benoit, P. (2012). "Net Section Tension Capacity of Bolted Connections in Cold-Reduced Steel Sheets". *Journal of Structural Engineering,* 138**,** 337-344.

Teh Lip, H. and Gilbert Benoit, P. (2013a). "Net Section Tension Capacity of Cold-Reduced Sheet Steel Angle Braces Bolted at One Leg". *Journal of Structural Engineering,* 139**,** 328-337.

Teh Lip, H. and Gilbert Benoit, P. (2013b). "Net Section Tension Capacity of Cold-Reduced Sheet Steel Channel Braces Bolted at the Web". *Journal of Structural Engineering,* 139**,** 740-747.

Uang, C. M., Sato, A., Hong, J. K. and Wood, K. (2010). "Cyclic Testing and Modeling of Cold-Formed Steel Special Bolted Moment Frame Connections". *Journal of Structural Engineering,* 136**,** 953-960.

Walker, A. C. (1975). "Design and analysis of cold-formed sections". *Halsted Press*.

Ye, J., Becque, J., Hajirasouliha, I., Mojtabaei, S. M. and Lim, J. B. P. (2018a). "Development of optimum cold-formed steel sections for maximum energy dissipation in uniaxial bending". *Engineering Structures,* 161**,** 55-67.

Ye, J., Mojtabaei, S. M. and Hajirasouliha, I. (2018b). "Local-flexural interactive buckling of standard and optimised cold-formed steel columns". *Journal of Constructional Steel Research,* 144**,** 106-118.

Ye, J., Mojtabaei, S. M. and Hajirasouliha, I. (2019). "Seismic performance of cold-formed steel bolted moment connections with bolting friction-slip mechanism". *Journal of Constructional Steel Research,* 156**,** 122-136.

Ye, J., Mojtabaei, S. M., Hajirasouliha, I. and Pilakoutas, K. (2020). "Efficient design of cold-formed steel bolted-moment connections for earthquake resistant frames". *Thin-Walled Structures,* 150.

Ye, J., Mojtabaei, S. M., Hajirasouliha, I., Shepherd, P. and Pilakoutas, K. (2018c). "Strength and deflection behaviour of cold-formed steel back-to-back channels". *Engineering Structures,* 177**,** 641-654.

Young, B. and Hancock, G. (2001). "Design of Cold-Formed Channels Subjected to Web Crippling". *J. Struct. Eng.,* 127(10)**,** 1137-1144.

List of tables

Table 1. Comparison between the flexural capacity of connections obtained from tests (Lim and Nethercot, 2003) and FE models

connection (*)	l_b (mm)	l_b/h	M_{max}^{exp} (kN.m)	M_{max}^{FE} (kN.m)	$M_{max}^{FE}/M_{max}^{exp}$
A	315	0.94	75	76.01	1.01
B	390	1.16	77.5	80.72	1.04
C	465	1.38	82.5	82.5	1.00
D	615	1.83	87.5	88.02	1.01
Average					1.02
St. dev					0.018

(*) with reference to (Mojtabaei et al., 2020)

Table 2. Eccentricity, slenderness and compressive capacity of CFS back-to-back sections

Cross-sections	X (mm)	t (mm)	λ_w	P_u (kN)
Ch.1	11.11	1	300	37.89
		2	150	127.24
		4	75	343.27
		6	50	679.89
Ch.2	15.71	1	250	40.12
		2	125	134.10
		4	62.5	408.16
		6	41.67	734.77
Ch.3	20.83	1	250	42.61
		2	125	142.65
		4	62.5	447.38
		6	41.67	798.71
Ch.4	23.44	1	200	45.75
		2	100	151.63
		4	50	454.86
		6	33.33	749.36
Ch.5	33.33	1	200	50.54
		2	100	167.85
		4	50	487.33
		6	33.33	827.57

Table 3. Proposed reduction factors for different bolt group configurations

Equation	Bolt group configuration	R_{pred}/R_{FE} Average	R_{pred}/R_{FE} Standard deviation
(Eq. 9)	2x2	1.007	0.03
(Eq. 10)	3x3	1.004	0.03
(Eq. 11)	4x4	1.001	0.03

Table 4. Statistical distributions used in reliability analysis

Variable	Distribution	Nominal	Mean	SD	COV	References
E	Normal	E	E	$0.03E$	0.03	Young et al. (Young and Hancock, 2001)
f_y	Lognormal	f_y	$1.1f_y$	$0.0693f_y$	0.063	Young et al. (Young and Hancock, 2001)
t	Normal	t	t	$0.005t$	0.005	Meza et al. (Meza et al., 2020)
h	Normal	h	h	$0.005h$	0.005	Meza et al. (Meza et al., 2020)
b	Normal	b	b	$0.002b$	0.002	Meza et al. (Meza et al., 2020)
c	Normal	c	c	$0.02c$	0.02	Meza et al. (Meza et al., 2020)

Table 5. Reliability calculations according to Eurocode

Loading	b_1	b_2	$V_{\delta 1}$	$V_{\delta 2}$	V_{rt}	$Q_{\delta 1}$	$Q_{\delta 2}$	Q_{rt}	Q	γ
P (Eqs. 9-11)	1.11	0.99	0.05	0.02	0.05	0.05	0.02	0.05	0.07	1.05
P (Eq. 12)	1.11	0.99	0.05	0.02	0.05	0.05	0.02	0.05	0.07	1.05
M + V (Eq. 24)	1.29	0.99	0.08	0.02	0.05	0.08	0.02	0.05	0.10	1.02
P + M + V (Eq. 26)	1.38	0.99	0.12	0.02	0.07	0.12	0.02	0.07	0.14	1.05

Table 6. Reliability calculations according to Eurocode without accounting for shear

Loading	b_1	b_2	$V_{\delta 1}$	$V_{\delta 2}$	V_{rt}	$Q_{\delta 1}$	$Q_{\delta 2}$	Q_{rt}	Q	γ
M + V (Eq. 46)	1.32	0.99	0.08	0.02	0.06	0.08	0.02	0.06	0.1	1.00
P + M + V (Eq. 27)	1.43	0.99	0.1	0.02	0.06	0.10	0.02	0.07	0.12	0.98

Table 7. Resistance factors for various types of loading for use with AISI design rules

Loading		V_{p1}	ϕ
P (EW)	(Eqs. 9-11)	0.11	0.98
P (DSM)	(Eqs. 9-11)	0.05	1.03
M + V	(Eq. 24)	0.15	1.01
P + M + V	(Eq. 26)	0.24	1.00
M + V	(Eq. 46)	0.08	1.00
P + M + V	(Eq. 27)	0.12	1.00
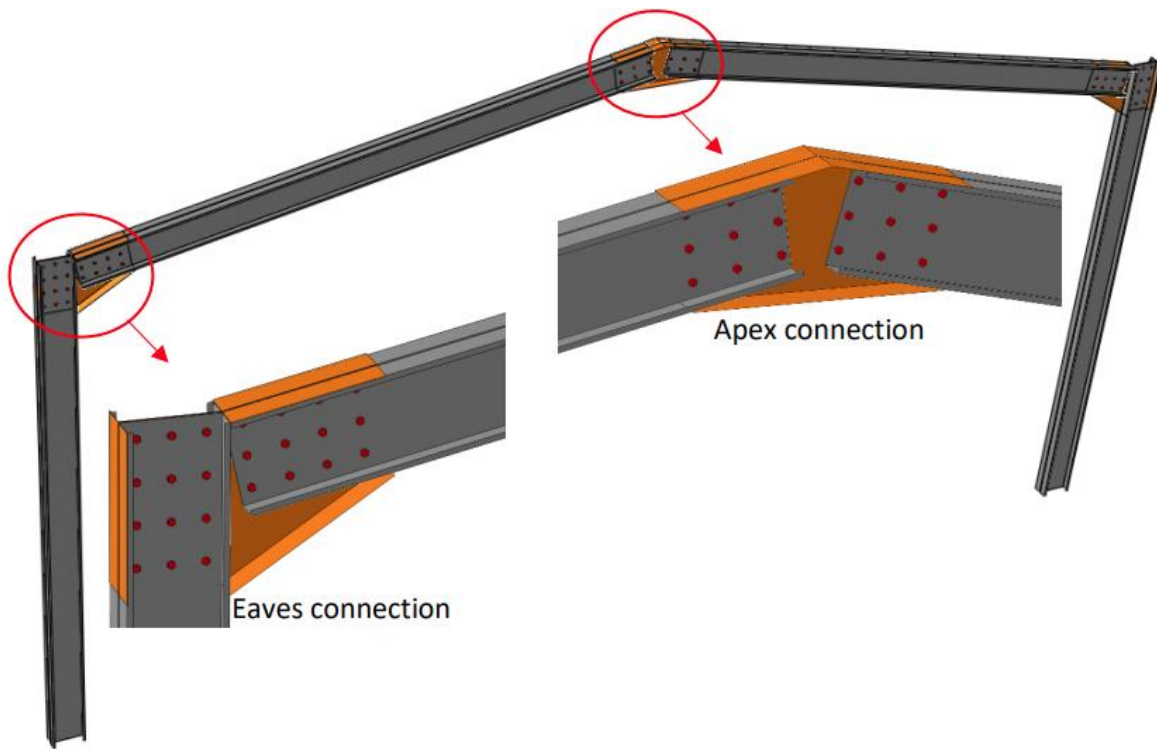
Fig. 1. Typical CFS frame used in practice
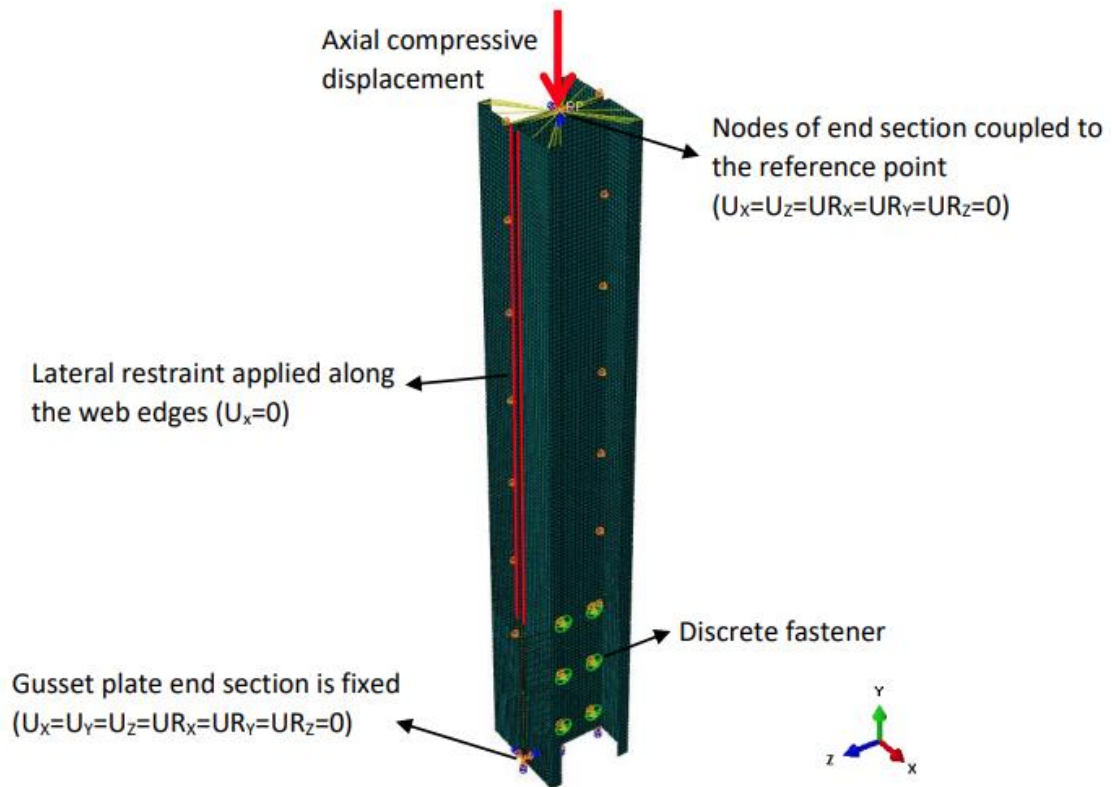
Fig. 2. FE model of bolted connection under pure compression
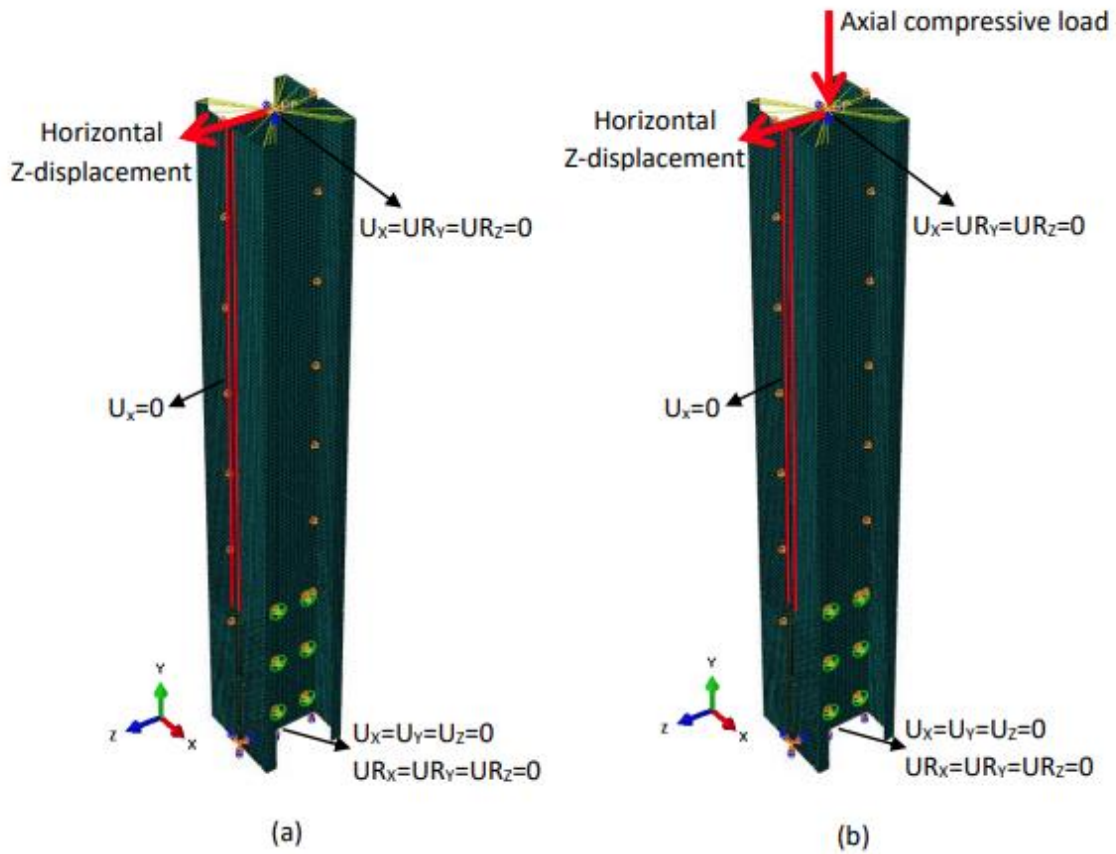
Fig. 3. FE models of bolted connection under combined (a) bending and shear and (b) bending, shear and compression
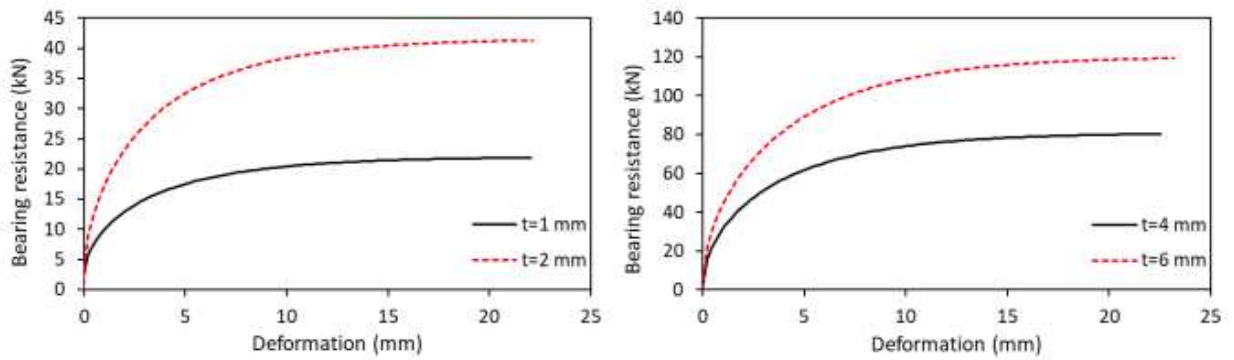
Fig. 4. Bearing behaviour of bolt against steel plate according to Fisher's equation
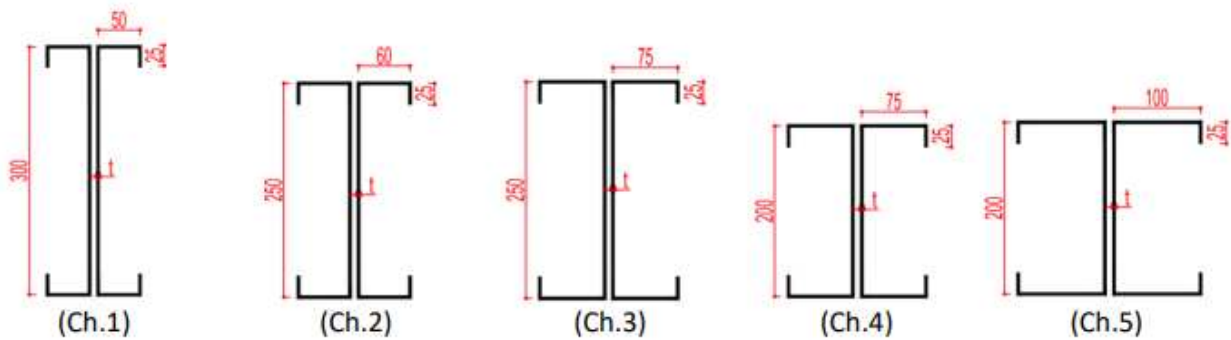
Fig. 5. Cross-sectional dimensions of beams in parametric studies
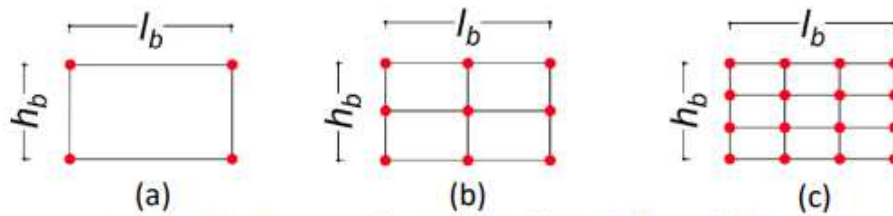
Fig. 6. Bolt group configurations: (a) 2x2, (b) 3x3, (c) 4x4
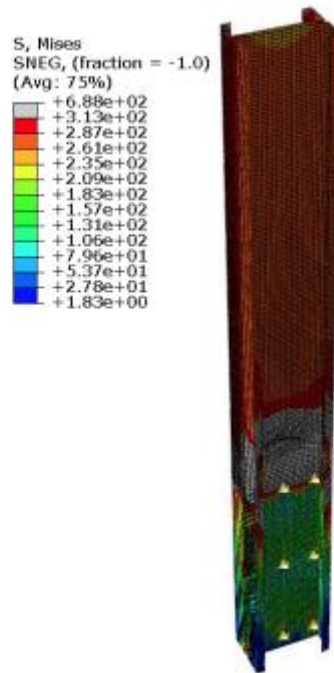
Fig. 7. Typical failure mechanism in CFS bolted connections
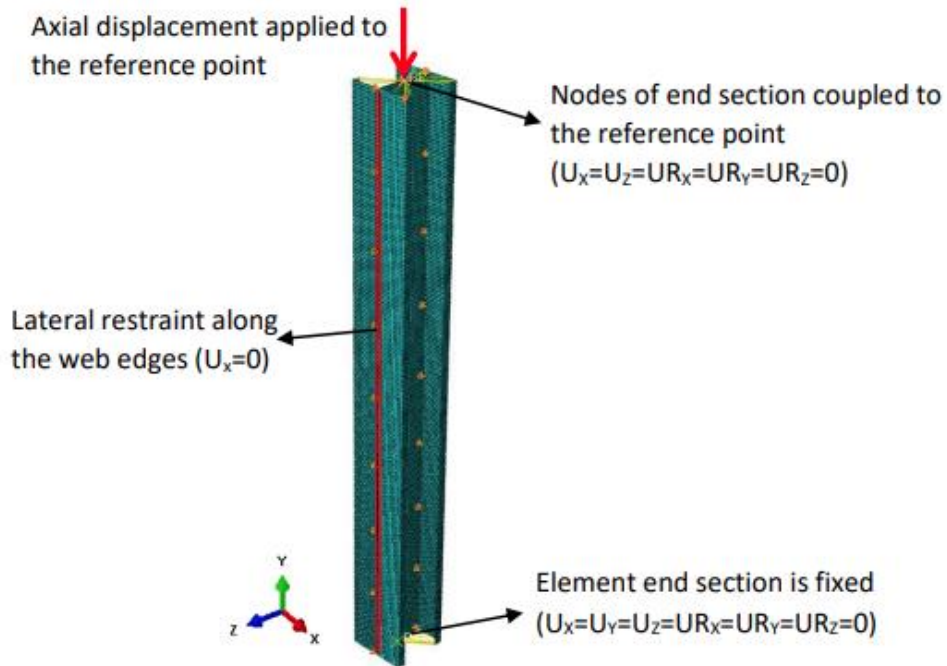
Fig. 8. FE model of CFS stub column to determine cross-sectional compressive capacity
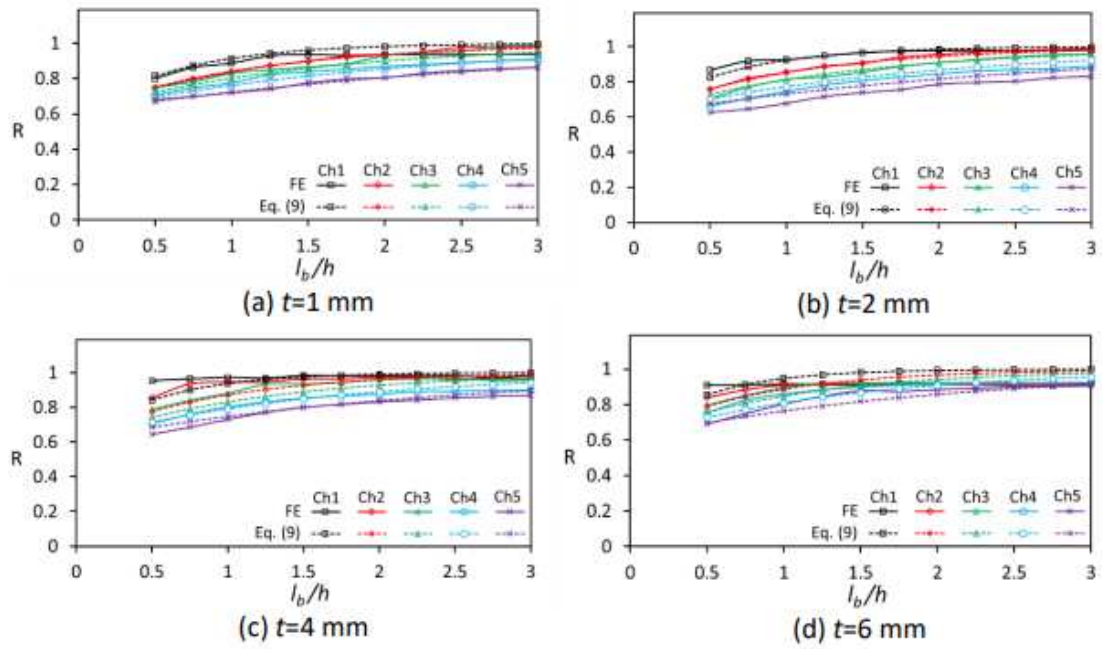
Fig. 9. Axial compressive capacity of CFS bolted connections with rectangular 2×2 bolt configuration and various bolt group lengths and cross-sectional geometries
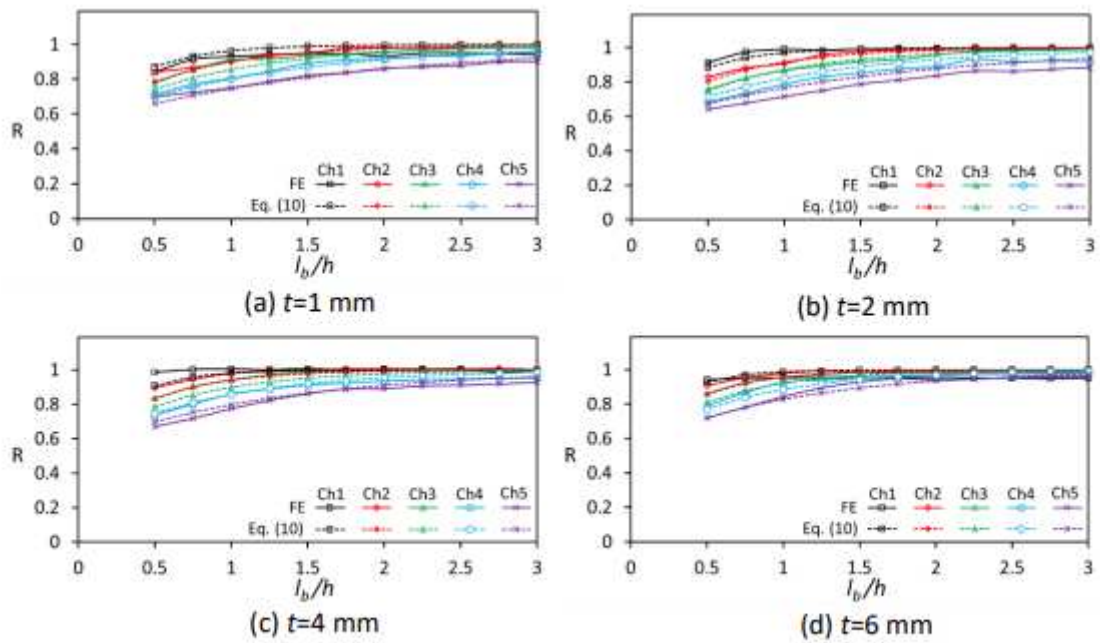
Fig. 10. Axial compressive capacity of CFS bolted connections with rectangular 3×3 bolt configuration and various bolt group lengths and cross-sectional geometries
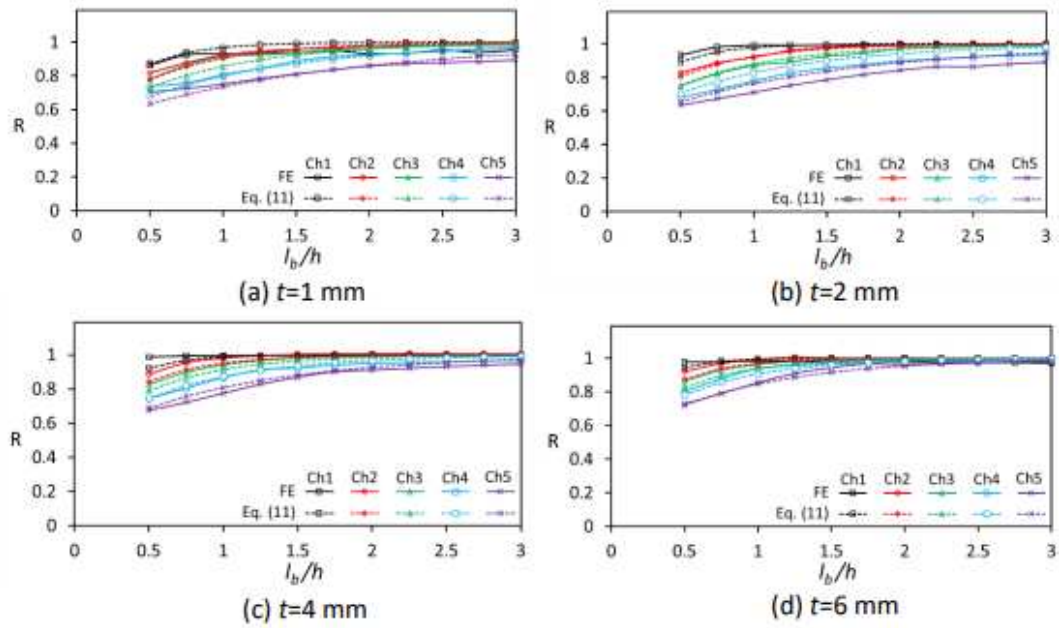
Fig. 11. Axial compressive capacity of CFS bolted connections with rectangular 4×4 bolt configuration and various bolt group lengths and cross-sectional geometries
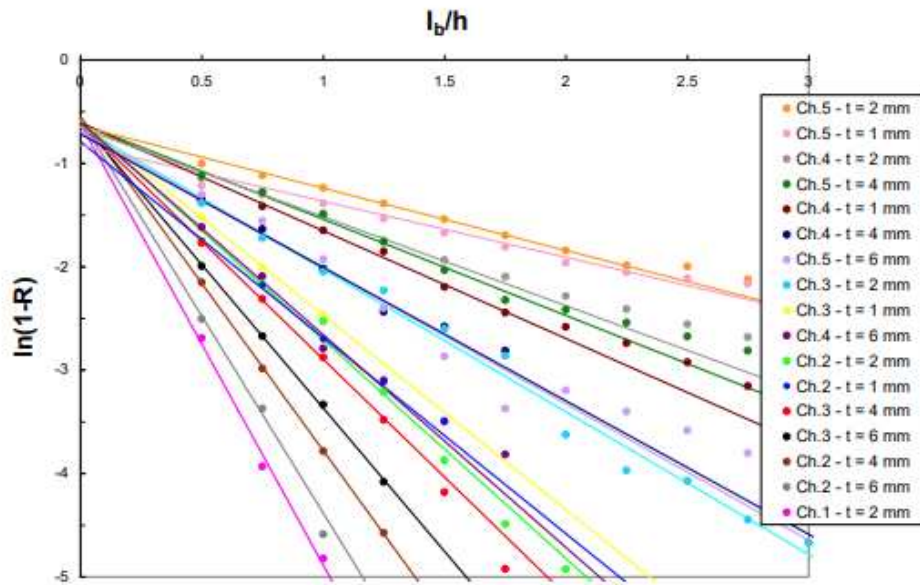
Fig. 12. Plot of $\ln(1-R)$ versus l_b/h for data pertaining to a 4×4 bolt group
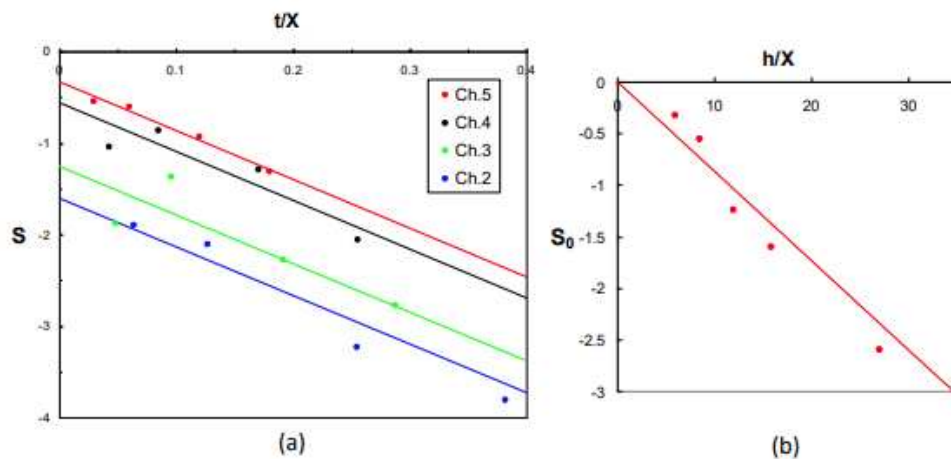
Fig. 13. Plots of (a) slope S vs. t/X and (b) intersection point S_0 vs. h/X

Channel type	Bolt group length	Thickness			
		1 mm	2 mm	4 mm	6 mm
Ch.1	$l_b/h = 0.5$				
	$l_b/h = 3$				
Ch.2	$l_b/h = 0.5$				
	$l_b/h = 3$				
Ch.3	$l_b/h = 0.5$				
	$l_b/h = 3$				
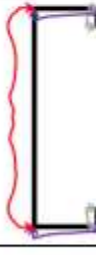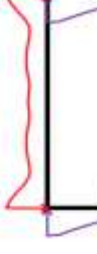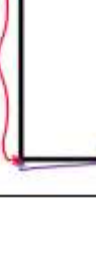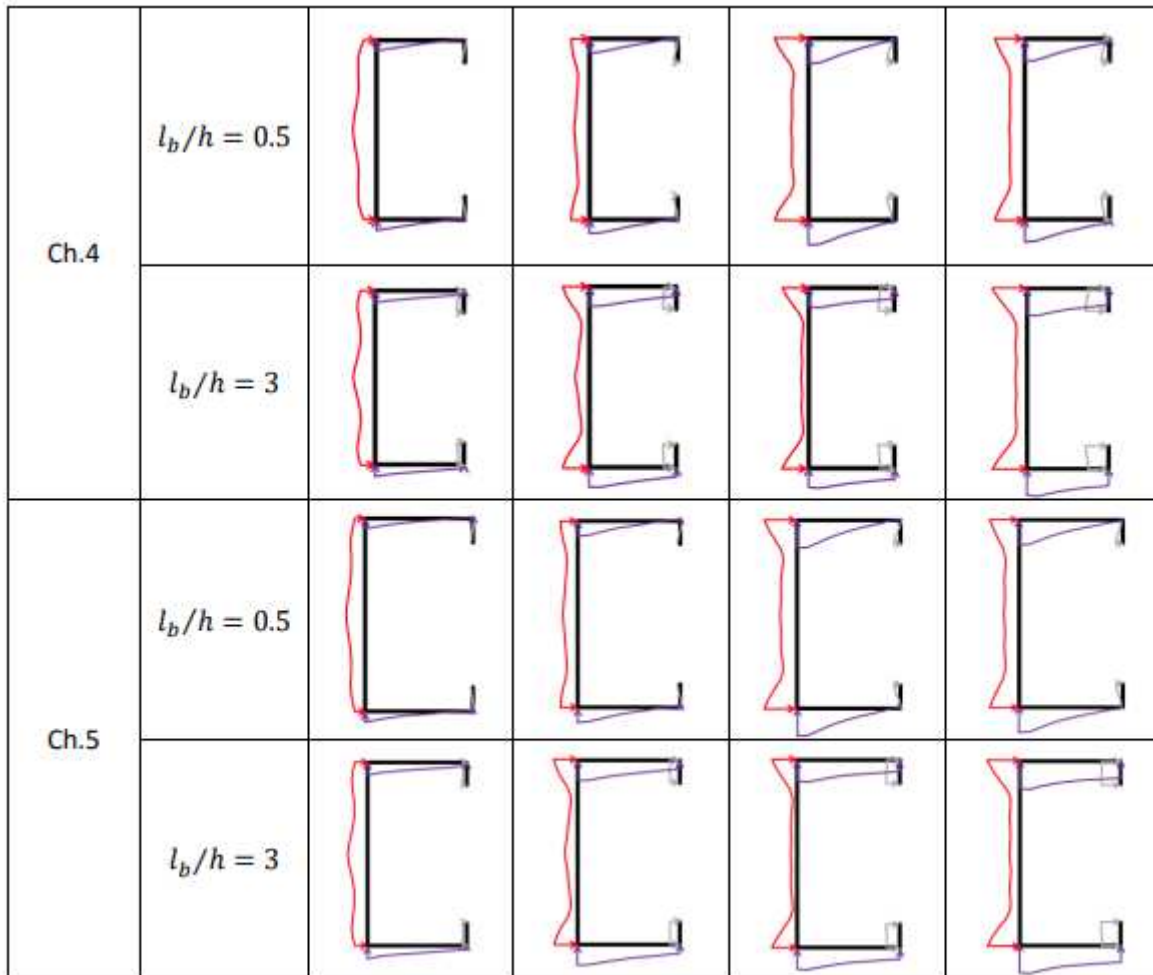
Fig. 14. FE elastic stress profile in CFS member for different bolt group lengths, thicknesses and cross-sectional geometries
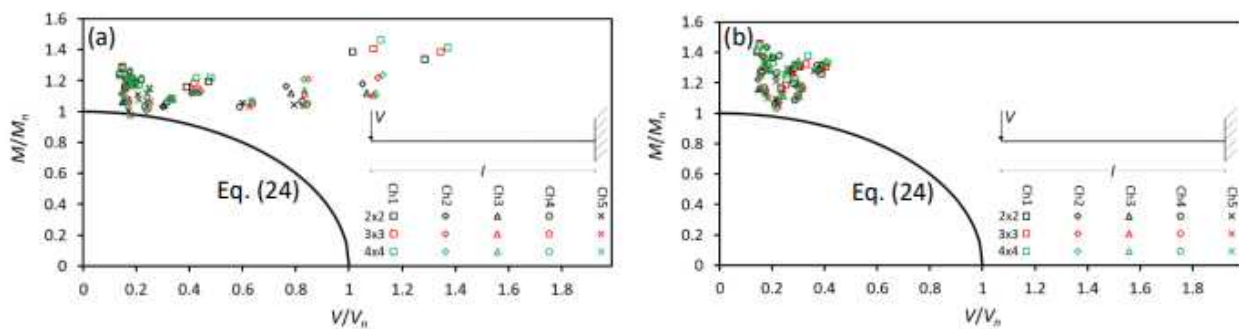
Fig. 15. Interaction diagram of M/M_n and V/V_n with V_n calculated according to (a) the AISI rules and (b) Eurocode 3
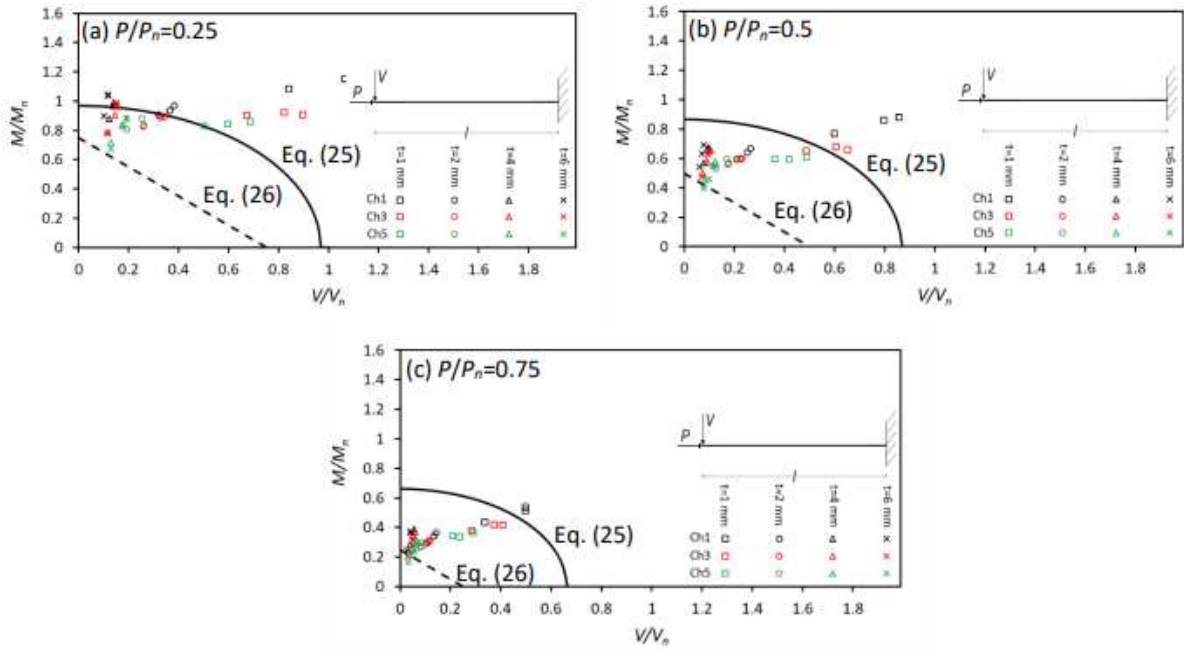
Fig. 16. Interaction between P/P_n, M/M_n and V/V_n in CFS bolted connections subject to compression, bending and shear force (using AISI standard)
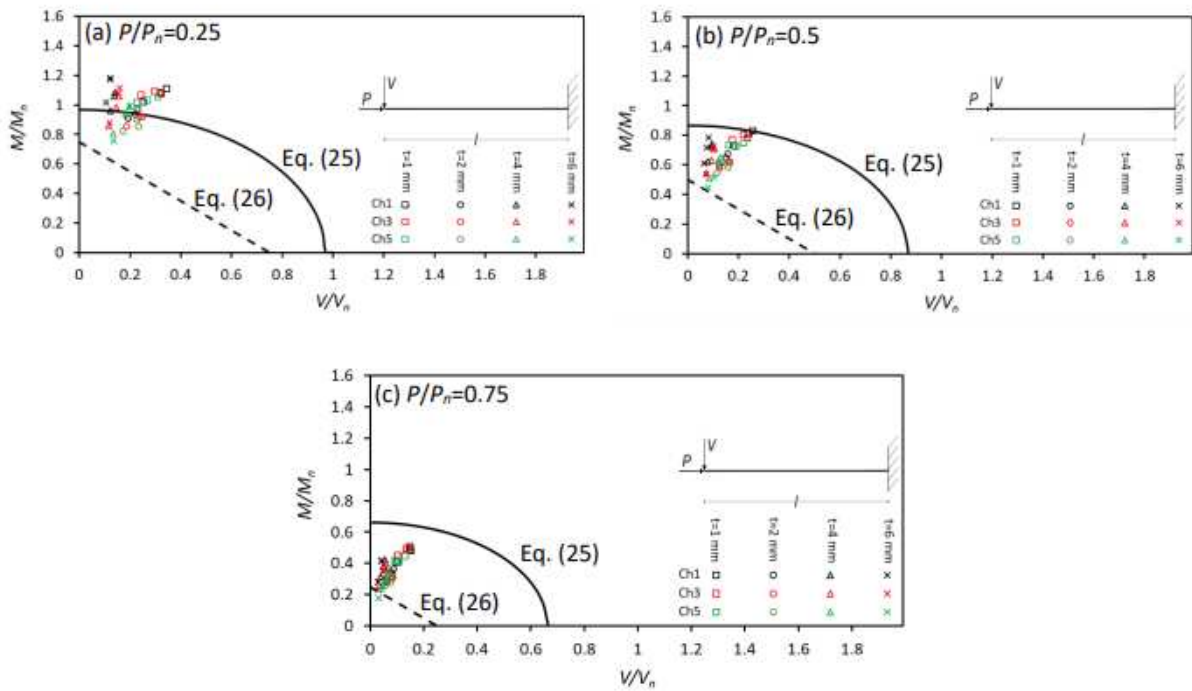
Fig. 17. Interaction between P/P_n, M/M_n and V/V_n in CFS bolted connections subject to compression, bending and shear force (using Eurocode 3)
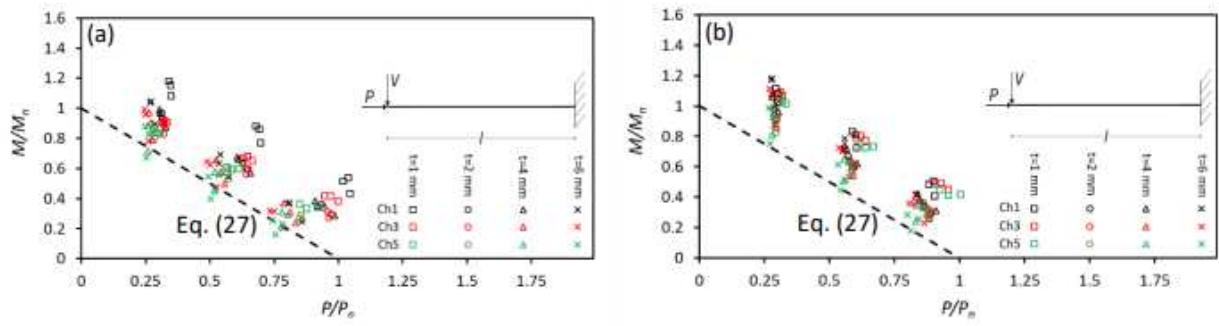
Fig. 18. Interaction between P/P_n and M/M_n in CFS bolted connections subject to compression, bending and shear force, using the (a) AISI and (b) Eurocode 3 design rules
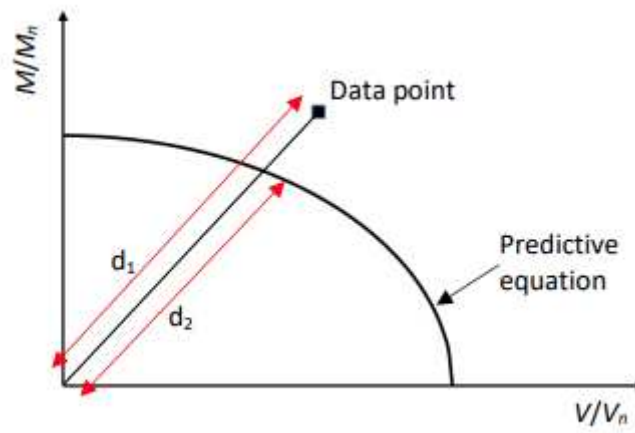
Fig. 19. Reliability approach for combined actions